Available online at www.sciencedirect.com
SCIENCE DIRECT®
ELSEVIER
International Journal of Solids and Structures 43 (2006) 2160–2173
INTERNATIONAL JOURNAL OF SOLIDS and STRUCTURES
www.elsevier.com/locate/ijsolstr

Crack growth resistance for anisotropic plasticity with non-normality effects

Viggo Tvergaard *, Brian Nyvang Legarth

Department of Mechanical Engineering, Solid Mechanics, Technical University of Denmark, DK-2800 Kgs. Lyngby, Denmark

Received 16 December 2004; received in revised form 18 April 2005
Available online 13 June 2005

Abstract

For a plastically anisotropic solid a plasticity model using a plastic flow rule with non-normality is applied to predict crack growth. The fracture process is modelled in terms of a traction–separation law specified on the crack plane. A phenomenological elastic–viscoplastic material model is applied, using one of two different anisotropic yield criteria to account for the plastic anisotropy, and in each case the effect of the normality flow rule is compared with the effect of non-normality. Conditions of small scale yielding are assumed, with mode I loading conditions far from the crack-tip, and various directions of the crack plane relative to the principal axes of the anisotropy are considered. It is found that the steady-state fracture toughness is significantly reduced when the non-normality flow rule is used. Furthermore, it is shown that the predictions are quite sensitive to the value of the maximum angle of deviation from normality in the non-normality flow rule.

Keywords: Anisotropic plasticity; Crack growth; Vertex; Finite strains

1. Introduction

A plasticity model using a vertex-type plastic flow rule on a smooth yield surface for an anisotropic solid has been proposed by Kuroda and Tvergaard (2001a). The model was proposed because of results found by using an abrupt strain path change to determine the shape of the subsequent yield surface in the vicinity of a current loading point (Kuroda and Tvergaard, 1999). The method was tested for polycrystal plasticity, based on the Taylor model for either f.c.c. or b.c.c. crystal structure, and the analyses show a clear non-normality of the small amount of plastic flow while the stress point moves along the yield surface. As

* Corresponding author. Tel.: +45 4525 4273; fax: +45 4593 1475.
E-mail address: viggo@mek.dtu.dk (V. Tvergaard).

0020-7683/$ - see front matter
doi:10.1016/j.ijsolstr.2005.04.012

has been discussed in detail by Kuroda and Tvergaard (1999), this apparent non-normality must be a vertex-type effect resulting from the Taylor model, since normality of each of the slip systems involved is an integral part of the crystal plasticity model. Also a corresponding experimental investigation for an aluminium alloy and a steel (Kuwabara et al., 2000) has shown a clear non-normality of the plastic strain rate vector relative to the stress path, which is regarded as part of the current yield surface.

During crack growth in metals the plastic work in the material surrounding the crack-tip contributes significantly to the fracture toughness, such that the macroscopic work of fracture is much larger than that of the local fracture process near the tip. This has been studied in a number of elastic–plastic crack growth computations (Tvergaard and Hutchinson, 1992, 1993; Tvergaard, 2001), with the local fracture process modelled by a traction–separation law along the crack plane having a specified work of separation per unit area and the surrounding material modelled by isotropic plasticity. This type of analysis has been used recently to investigate the effect of plastic anisotropy on predicted crack growth resistance curves (Tvergaard and Legarth, 2004).

The cause of plastic anisotropy is often texture development during large plastic straining, or in some cases the microstructure of the solid, where e.g. inclusions elongated in a particular direction will give anisotropic properties (Legarth, 2003). Some different models for anisotropic plasticity have been discussed by Kuroda and Tvergaard (2000) in the context of sheet metal formability, and Legarth et al. (2002a,b) have used the anisotropic yield surface of Hill (1948) to study crack-tip blunting prior to the onset of crack growth. Legarth et al. (2002a,b) found that the plastic zones around the crack-tip show strong non-symmetries for certain orientations of the principal axes of anisotropy relative to the crack plane.

In the crack growth analyses of Tvergaard and Legarth (2004) the anisotropic yield surface proposed by Hill (1948) or that proposed by Barlat et al. (1991) are used, with the usual normality of the plastic flow rule, and with the elastic–viscoplastic versions of the anisotropic material models, used in Kuroda and Tvergaard (2000). The crack growth analyses are here extended to consider the effect of the non-normality of the plastic flow rule found by Kuroda and Tvergaard (1999), since the vertex-type effect is expected to significantly reduce the resistance to the non-proportional stress paths that are characteristic around the tip of a growing crack. Apart from this, the analyses are based on the assumptions of small scale yielding as well as straight ahead crack growth, as in Tvergaard and Legarth (2004).

2. Problem formulation

2.1. Anisotropic plasticity model with non-normality

The constitutive model to be used here is that proposed by Kuroda and Tvergaard (2001a,b). Assuming small elastic and finite plastic deformations, the result of the Eulerian kinematics can be expressed by

$$\begin{aligned} \mathbf{D} &= \mathbf{D}^{\mathrm{e}} + \mathbf{D}^{\mathrm{p}} = \mathbf{D}^{\mathrm{e}} + \dot{\Phi}\mathbf{N}^{\mathrm{p}} \\ \mathbf{W} &= \boldsymbol{\omega} + \mathbf{W}^{\mathrm{p}} = \boldsymbol{\omega} + \dot{\Phi}\boldsymbol{\Omega}^{\mathrm{p}} \end{aligned} \tag{2.1}$$

Here $\mathbf{D}$ and $\mathbf{W}$ are the symmetric and anti-symmetric parts of the spatial velocity gradient $\mathbf{L}$ ($=\partial v_i/\partial x_j \mathbf{e}_i \otimes \mathbf{e}_j$ where $\mathbf{v}$ is the velocity of a material particle, $\mathbf{x}$ is the current position and $\mathbf{e}_i$ the Cartesian basis), the superscripts e and p denote elastic and plastic parts, respectively, $\boldsymbol{\omega}$ is the spin of the substructure, and $\mathbf{W}^{\mathrm{p}}$ is the plastic spin, while $\boldsymbol{\Omega}^{\mathrm{p}}$ is the direction of $\mathbf{W}^{\mathrm{p}}$. Here it is assumed that $\mathbf{W}^{\mathrm{p}} = 0$, so that $\mathbf{W} = \boldsymbol{\omega}$. The scalar-valued quantity $\dot{\Phi}$ is a non-negative overstress function for rate-dependent cases or a loading multiplier appearing as $\langle\lambda\rangle$ in rate-independent plasticity ($\langle\,\rangle$ are the Macauley brackets).

With the superposed o denoting an objective rate with respect to the spin $\boldsymbol{\omega}$ and the superposed dot denoting a material time derivative, the elasticity relation is assumed to be given by Hooke's law

$$\overset{\circ}{\boldsymbol{\sigma}} = \dot{\boldsymbol{\sigma}} - \boldsymbol{\omega}\boldsymbol{\sigma} + \boldsymbol{\sigma}\boldsymbol{\omega} = \mathbf{C} : \mathbf{D}^{\mathrm{e}} = \mathbf{C} : \mathbf{D} - \dot{\Phi}\mathbf{C} : \mathbf{N}^{\mathrm{p}} \tag{2.2}$$

where $\boldsymbol{\sigma}$ is the Cauchy stress and $\mathbf{C}$ is a fourth order isotropic elastic moduli tensor, determined by Young's modulus E and Poisson's ratio v.

For the anisotropic plasticity considered here, orthotropic symmetry is assumed. The structure variables to be considered are two types of quantities, the orthonormal unit vectors $\mathbf{n}_i$, and the equivalent plastic strain ε^{p}. The orthonormal vectors $\mathbf{n}_i$ are defined along the axes of orthotropy, $\hat{x}_i$, which evolve according to

$$\dot{\mathbf{n}}_i = \boldsymbol{\omega}\mathbf{n}_i \tag{2.3}$$

since $\overset{\circ}{\mathbf{n}}_i \equiv \mathbf{0}$. The stress components with respect to the orthotropic axes, $\hat{x}_i$, are denoted by $(\hat{})$, thus $\hat{\sigma}_{ij} = \mathbf{n}_i \cdot \boldsymbol{\sigma} \cdot \mathbf{n}_j$ for $i, j = 1, 2, 3$, see Fig. 1. The initial angle of orientation of plastic anisotropy is denoted by θ_0.

A rate-dependent yield surface can be written as

$$f = J(\boldsymbol{\sigma}, \mathbf{n}_i, \varepsilon^{\mathrm{p}}) - K(g(\varepsilon^{\mathrm{p}}), \dot{\Phi}) = 0 \tag{2.4}$$

where J is an equivalent stress for which the functional form can be motivated by a rate-independent theory of plasticity, K is a scalar variable representing a strain-rate-sensitive stress magnitude, and $g(\varepsilon^{\mathrm{p}})$ is a strain hardening function which portrays isotropic hardening. This function is taken to follow a power law

$$g(\varepsilon^{\mathrm{p}}) = \boldsymbol{\sigma}_0 \left(1 + \frac{\varepsilon^{\mathrm{p}}}{\varepsilon_0}\right)^n \tag{2.5}$$

where σ_0 is the initial yield stress, ε_0 is a material constant and n is the strain hardening exponent. The J is assumed to be pressure insensitive, i.e. $\partial J/\partial \boldsymbol{\sigma} = \mathbf{N}^n$ is a deviatoric quantity. From Eq. (2.4) the expression for $\dot{\Phi}$ is determined as $\dot{\Phi} = \dot{\Phi}(J, g)$.

The unit outward normal $\mathbf{n}$ to the yield surface is given by

$$\mathbf{n} = \left(\frac{\partial J}{\partial \boldsymbol{\sigma}}\right) \Big/ \left\| \frac{\partial J}{\partial \boldsymbol{\sigma}} \right\| \tag{2.6}$$

where $\|(\bullet)\| = \sqrt{\mathrm{tr}[(\bullet)^{\mathrm{T}}(\bullet)]}$. A non-linear dependence of the plastic strain rate $\mathbf{D}^{\mathrm{p}}$ on the total strain rate $\mathbf{D}$ is assumed. Introducing the notation for a deviatoric quantity, $(\bullet)' = (\bullet) - (1/3)(\mathbf{I} \otimes \mathbf{I}) : (\bullet)$, with the unity tensor $\mathbf{I}$, a direction $\mathbf{m}$ normal to $\mathbf{n}$ is defined as

$$\mathbf{m} = \frac{\mathbf{D}' - (\mathbf{n} : \mathbf{D}')\mathbf{n}}{\|\mathbf{D}' - (\mathbf{n} : \mathbf{D}')\mathbf{n}\|} \tag{2.7}$$

Then, the direction $\mathbf{N}^{\mathrm{p}}$ of the plastic strain rate $\mathbf{D}^{\mathrm{p}}$ is taken to be

$$\mathbf{N}^{\mathrm{p}} = \mathbf{n} + \hat{\delta}\mathbf{m} \tag{2.8}$$

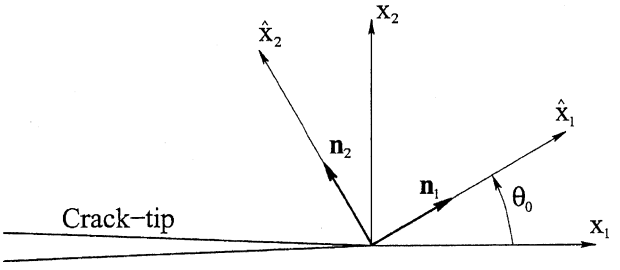

Fig. 1. Definition of the orthonormal basis of plastic anisotropy.

where $\hat{\delta}$ is a scalar-valued function to be specified below. Then, (2.8) together with (2.1), i.e. $\mathbf{D}^{\mathrm{p}} = \dot{\Phi}\mathbf{N}^{\mathrm{p}}$, specifies the plasticity model with the vertex-type effect (Simo, 1987), which expresses the non-normality of the plastic flow. The equivalent plastic strain ε^{p} is defined as

$$\varepsilon^{\mathrm{p}} = \int \dot{\varepsilon}^{\mathrm{p}}\,\mathrm{d}t = \int \sqrt{2/3}\dot{\Phi}\,\mathrm{d}t \tag{2.9}$$

The value of $\hat{\delta}$ is taken to be given by (Kuroda and Tvergaard, 2001a,b,c)

$$\hat{\delta} = \tan\psi^{\mathrm{p}}, \quad \psi^{\mathrm{p}} = \begin{cases} \alpha\psi & \text{for } \alpha\psi \leqslant \psi^{\mathrm{p}}_{\mathrm{crit}} \\ \psi^{\mathrm{p}}_{\mathrm{crit}} & \text{for } \alpha\psi > \psi^{\mathrm{p}}_{\mathrm{crit}} \end{cases} \tag{2.10}$$

$$\psi = \cos^{-1}\left[\frac{\mathbf{n} : \mathbf{D}'}{\|\mathbf{D}'\|}\right], \quad \alpha = \frac{1}{cg/\mu + 1} \tag{2.11}$$

where c is a coefficient, which governs non-coaxiality between $\mathbf{D}'$ and $\mathbf{D}^{\mathrm{p}}$, and $\mu = E/\{2(1+\nu)\}$ is the elastic shear modulus. The ratio μ/g represents the elastic modulus normalised by the current stress level g according to strain hardening. For usual elastic–viscoplastic materials α is close to unity, but a small deviation from unity has a large effect on predictions of strain localization (Kuroda and Tvergaard, 2001a,c). It is noted that when $\psi^{\mathrm{p}}_{\mathrm{crit}} \to 0$ the present plasticity model reduces to the normality flow rule.

In the present analyses, the following strain-rate hardening law is used in Eq. (2.4)

$$K\big(g(\varepsilon^{\mathrm{p}}), \dot{\Phi}\big) \equiv g(\varepsilon^{\mathrm{p}})\left(\frac{\dot{\Phi}}{\dot{\Phi}_0}\right)^m \tag{2.12}$$

where $\dot{\Phi}_0$ is a material constant having the dimension of $(\text{time})^{-1}$ and m is the strain-rate sensitivity exponent.

Plastic anisotropy is accounted for by using two different phenomenological theories, namely Hill (1948, 1950), which is quadratic in terms of the stress components, and the non-quadratic proposal by Barlat et al. (1991), subsequently referred to as Hill-48 and Barlat-91, respectively.

For the non-associated model (2.8), in presence of anisotropy, there is the possibility that the plastic work rate is negative, even for $\psi^{\mathrm{p}}_{\mathrm{crit}} < \pi/2$. The angle $\psi^{\mathrm{p}}_{\mathrm{crit}}$ should not exceed $\pi/2 - \psi_{\mathrm{n}\sigma'}$, where $\psi_{\mathrm{n}\sigma'}$ is the angle between the normal and the stress deviator at the current point on the yield surface. This requirement will be satisfied for moderate intensity of anisotropy and moderate $\psi^{\mathrm{p}}_{\mathrm{crit}}$. The maximum allowable value of $\psi^{\mathrm{p}}_{\mathrm{crit}}$ has been calculated numerically for the particular parameter values used in the two yield criteria to be considered here. The values are about 54° for Hill-48 and 64° for Barlat-91, and thus the value $\psi^{\mathrm{p}}_{\mathrm{crit}} = 20°$ to be used in some of the present computations is well within the limits.

Hill-48: The classical quadratic yield criterion proposed by Hill (1948, 1950) is

$$\begin{aligned} J &= \sqrt{\frac{3}{2(F+G+H)}}\big[F(\hat{\sigma}_{22}-\hat{\sigma}_{33})^2 + G(\hat{\sigma}_{33}-\hat{\sigma}_{11})^2 + H(\hat{\sigma}_{11}-\hat{\sigma}_{22})^2 + 2N\hat{\sigma}_{12}^2 + 2L\hat{\sigma}_{23}^2 + 2M\hat{\sigma}_{13}^2\big]^{1/2} \\ &\quad - C_1 g(\varepsilon^{\mathrm{p}})\left(\frac{\dot{\Phi}}{\dot{\Phi}_0}\right)^m = 0 \\ C_1 &= \sqrt{\frac{3(G+H)}{2(F+G+H)}} \end{aligned} \tag{2.13}$$

For $F = G = H = 1$ and $N = L = M = 3$ this yield function simplifies to the isotropic von Mises yield criterion. For plane strain conditions, where $\hat{\sigma}_{13} = \hat{\sigma}_{23} = 0$, the two coefficients of anisotropy M and L are left out of the considerations.

Barlat-91: Based on the work of Hershey (1954) and Hosford (1972), Barlat et al. (1991) proposed the higher order yield function

$$J = \left(\frac{\Psi}{2}\right)^{\frac{1}{d}} - g(\varepsilon^{\mathrm{p}})\left(\frac{\dot{\Phi}}{\dot{\Phi}_0}\right)^m = 0$$
$$\Psi = [S_1 - S_2]^d + [S_2 - S_3]^d + [S_1 - S_3]^d \tag{2.14}$$

where (see Barlat et al., 1997)

$$S_1 = 2\sqrt{I_2}\cos\left(\frac{\bar{\theta}}{3}\right), \quad S_2 = 2\sqrt{I_2}\cos\left(\frac{\bar{\theta}-2\pi}{3}\right), \quad S_3 = 2\sqrt{I_2}\cos\left(\frac{\bar{\theta}+2\pi}{3}\right) \tag{2.15}$$

$$I_2 = \frac{1}{3}[(\bar{f}\bar{F})^2 + (\bar{g}\bar{G})^2 + (\bar{h}\bar{H})^2] + \frac{1}{54}[(\bar{a}\bar{A} - \bar{c}\bar{C})^2 + (\bar{c}\bar{C} - \bar{b}\bar{B})^2 + (\bar{b}\bar{B} - \bar{a}\bar{A})^2]$$
$$I_3 = \frac{1}{54}[(\bar{c}\bar{C} - \bar{b}\bar{B})(\bar{a}\bar{A} - \bar{c}\bar{C})(\bar{b}\bar{B} - \bar{a}\bar{A})] + \bar{f}\bar{g}\bar{h}\bar{F}\bar{G}\bar{H} - \frac{1}{6}[(\bar{c}\bar{C} - \bar{b}\bar{B})(\bar{f}\bar{F})^2$$
$$+ (\bar{a}\bar{A} - \bar{c}\bar{C})(\bar{g}\bar{G})^2 + (\bar{b}\bar{B} - \bar{a}\bar{A})(\bar{h}\bar{H})^2] \tag{2.16}$$

$$0 \leqslant \bar{\theta} = \arccos\left(\frac{I_3}{I_2^{3/2}}\right) \leqslant \pi \tag{2.17}$$

with

$$\bar{A} = \hat{\sigma}_{22} - \hat{\sigma}_{33}; \quad \bar{F} = \hat{\sigma}_{23}$$
$$\bar{B} = \hat{\sigma}_{33} - \hat{\sigma}_{11}; \quad \bar{G} = \hat{\sigma}_{31} \tag{2.18}$$
$$\bar{C} = \hat{\sigma}_{11} - \hat{\sigma}_{22}; \quad \bar{H} = \hat{\sigma}_{12}$$

For $\bar{\theta} = 0$ or $\bar{\theta} = \pi$ in Eq. (2.17) the derivatives $\partial J/\partial\sigma$ are singular. For these particular cases Eq. (2.14) reduces to

$$\Phi = 2 \cdot 3^d I_2^{\frac{d}{2}} \quad \text{for } \bar{\theta} = 0 \text{ or } \bar{\theta} = \pi \tag{2.19}$$

which are then directly used to evaluate the strain increments. If the coefficients of anisotropy, $\bar{a}$, $\bar{b}$, $\bar{c}$, $\bar{f}$, $\bar{g}$ and $\bar{h}$, are chosen to be unity and the exponent to $d = 2$, this criterion reduces to the von Mises yield surface. For plane strain computations the two coefficients $\bar{f}$ and $\bar{g}$ are irrelevant.

2.2. Cohesive zone model

A traction–separation law proposed by Needleman (1987) for separation due to the normal stress on an interface was generalized by Tvergaard (1990) to also account for separation due to tangential stresses. A special version of this generalized model, for which the traction–separation law is governed by a potential, was used by Tvergaard and Hutchinson (1993). Here, δ_{n} and δ_{t} denote the normal and tangential components of the relative displacement of the crack faces across the interface in the zone where the fracture processes are occurring (Fig. 2). When δ_{n}^c and δ_{t}^c are critical values of these displacement components and a single non-dimensional separation measure is defined as $\lambda = [(\delta_{\mathrm{n}}/\delta_{\mathrm{n}}^c)^2 + (\delta_{\mathrm{t}}/\delta_{\mathrm{t}}^c)^2]^{1/2}$ the tractions drop to zero at $\lambda = 1$. With $\sigma(\lambda)$ displayed in Fig. 2, a potential from which the tractions are derived is defined as

$$\Phi(\delta_{\mathrm{n}}, \delta_{\mathrm{t}}) = \delta_{\mathrm{n}}^c \int_0^{\lambda} \sigma(\lambda')\,\mathrm{d}\lambda' \tag{2.20}$$

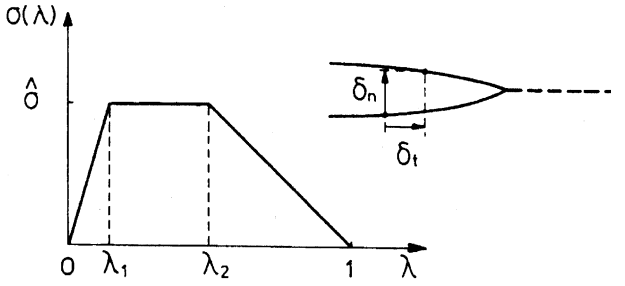

Fig. 2. Specification of traction–separation relation.

The normal and tangential components of the tractions acting on the interface in the fracture process zone are given by

$$T_{\mathrm{n}} = \frac{\partial \Phi}{\partial \delta_{\mathrm{n}}} = \frac{\sigma(\lambda)}{\lambda}\frac{\delta_{\mathrm{n}}}{\delta_{\mathrm{n}}^{c}}, \quad T_{\mathrm{t}} = \frac{\partial \Phi}{\partial \delta_{\mathrm{t}}} = \frac{\sigma(\lambda)}{\lambda}\frac{\delta_{\mathrm{t}}}{\delta_{\mathrm{t}}^{c}}\frac{\delta_{\mathrm{n}}^{c}}{\delta_{\mathrm{t}}^{c}} \tag{2.21}$$

The peak normal traction under pure normal separation is $\hat{\sigma}$, and the peak shear traction is $\left(\delta_{\mathrm{n}}^{c}/\delta_{\mathrm{t}}^{c}\right)\hat{\sigma}$ in a pure tangential separation. The work of separation per unit area of interface is given by Eq. (2.20) with $\lambda = 1$, and for the separation function $\sigma(\lambda)$ in Fig. 2 the work is

$$\Gamma_0 = \frac{1}{2}\hat{\sigma}\delta_{\mathrm{n}}^{c}(1 - \lambda_1 + \lambda_2) \tag{2.22}$$

It has been found by Tvergaard and Hutchinson (1992, 1993) that the details of the shape of the separation law are not very important, and that the two most important parameters characterizing the fracture process in this model are Γ_0 and $\hat{\sigma}$.

2.3. Small scale yielding formulation

The numerical computations for conditions of small scale yielding are carried out for a circular region with initial radius A_0. Plane strain conditions and remote mode I loading are assumed. The x_1-axis is in the crack plane and the initial crack-tip is located at $x_1 = x_2 = 0$ (see Fig. 3). The traction–separation relation

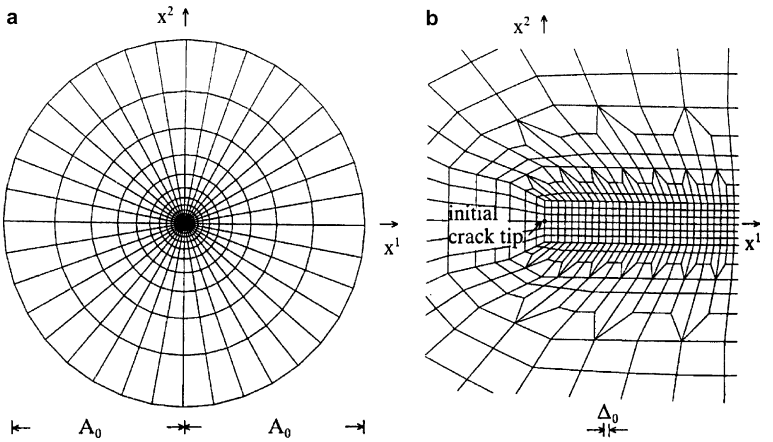

Fig. 3. Mesh used for some of the crack growth analyses.

used to model the fracture process (Fig. 2) is specified everywhere on the boundary $x_1 > 0$, $x_2 = 0$ of the region analysed, while zero tractions are specified for $x_1 \leqslant 0$, $x_2 = 0$.

According to the small strain linear elastic solution the in-plane stress components near the crack-tip are of the form

$$\sigma_{\alpha\beta} = \frac{K}{\sqrt{2\pi r}} f_{\alpha\beta}(\theta) \tag{2.23}$$

for mode I loading, where (r, θ) are polar coordinates and K is the amplitude of the singular stress field. The displacements are specified on the outer semicircular boundary according to the singular K-field solution around the crack-tip. Thus, the loading is applied by incrementally increasing the amplitude K for the displacements on the semicircular boundary. The value of the J-integral has been calculated on a number of contours around the crack-tip and good agreement with the prescribed amplitude K of the edge displacements has been found.

Two reference quantities K_0 and R_0 are introduced for the presentation of the results

$$K_0 = [E\Gamma_0/(1-\nu^2)]^{1/2} \tag{2.24}$$

$$R_0 = \frac{1}{3\pi}\left(\frac{K_0}{\sigma_0}\right)^2 = \frac{1}{3\pi}\frac{E\Gamma_0}{(1-\nu^2)\sigma_0^2} \tag{2.25}$$

Here, K_0 represents the mode I stress intensity factor needed to advance the crack when plastic dissipation is negligible, i.e. the stress intensity factor needed to supply just the work of the fracture process Γ_0. The reference length R_0 scales with the size of the plastic zone when $K \cong K_0$.

2.4. Numerical procedure

The numerical crack growth procedure follows that of Tvergaard and Legarth (2004). Thus, the finite-element solution is carried out in the context of an updated Lagrangian formulation (McMeeking and Rice, 1975) based on the principle of virtual work. Disregarding body forces the incremental form of the principle of virtual work in terms of the first Piola–Kirchhoff stress, $s_{ij} \neq s_{ji}$, is (Yamada and Hirakawa, 1978; Tvergaard, 1990; Yamada and Sasaki, 1995)

$$\begin{aligned}\Delta t \int_V \dot{s}_{ij}\delta v_{j,i}\,\mathrm{d}V + \Delta t \int_{S_I} \{\dot{T}_\mathrm{n}\delta(\dot{\delta}_\mathrm{n}) + \dot{T}_\mathrm{t}\delta(\dot{\delta}_\mathrm{t})\}\,\mathrm{d}S \\ = \Delta t \int_S \dot{T}_i \delta v_i\,\mathrm{d}S - \left[\int_V s_{ij}\delta v_{j,i}\,\mathrm{d}V - \int_S T_i\delta v_i\,\mathrm{d}S + \int_{S_I}\{T_\mathrm{n}\delta(\dot{\delta}_\mathrm{n}) + T_\mathrm{t}\delta(\dot{\delta}_\mathrm{t})\}\,\mathrm{d}S\right]\end{aligned} \tag{2.26}$$

where $T_i = s_{ji}n_j$, V is the volume, S is the surface and S_I denotes the debonding interface, T_i are the nominal tractions and δv_i are the virtual velocities in the current deformed configuration. Therefore, s_{ij} is identical to σ_{ij}, but $\dot{s}_{ij}$ is not equal to $\dot{\sigma}_{ij}$, i.e. $\dot{\boldsymbol{s}} = \dot{\boldsymbol{\sigma}} - \boldsymbol{L}\boldsymbol{\sigma} + \mathrm{tr}(\boldsymbol{L})\boldsymbol{\sigma}$. The bracketed terms in Eq. (2.26) are equilibrium correction terms.

An example of the mesh used for the computations is shown in Fig. 3. A uniform mesh region is used in the range where crack growth is studied with the length of one square element denoted by Δ_0, and the initial crack-tip is located at $x^1 = 0$. The elements used are quadrilaterals each built-up of four triangular, linear displacement elements, and 120×6 quadrilaterals are used in the uniform mesh along the interface. These crossed triangles are known to have good accuracy in elastic–plastic problems, as they avoid locking due to near incompressibility (Nagtegaal et al., 1974). The outer radius of the region analysed is chosen to be $A_0/\Delta_0 = 800000$, in order that the plastic zone size should not exceed $A_0/10$.

The boundary conditions prescribed on the outer edge are the displacements corresponding to the singular K-field. During the initial part of the crack growth resistance curve an increment of K is prescribed,

but when K approaches its asymptote, a Rayleigh–Ritz finite-element method (Tvergaard, 1976) is needed to ensure a monotonic increase in displacement differences across the crack tip. In each increment the time step, Δt, for the next increment is corrected according to $(\dot{\varepsilon}^{\mathrm{p}})_{\max} \cdot \Delta t \leqslant c_1$ and $(\dot{\lambda})_{\max} \cdot \Delta t \leqslant c_2$, where the label *max* refers to the maximum effective plastic strain rate in any triangular element, or the maximum rate of the debonding separation measure λ, at the current increment. The values of the constants c_1 and c_2 are in several computations chosen as $c_1 = 0.02$ and $c_2 = 0.004$, but in some cases smaller values of the constants have been needed, to avoid numerical instabilities.

In the crack growth solutions it is known (Tvergaard and Hutchinson, 1992) that good numerical convergence is obtained if the length of the process region exceeds two to three times Δ_0. This is ensured in the present analyses.

3. Results

The crack growth analyses here, for materials with the non-normality flow rule, consider the same two anisotropic metals studied in Tvergaard and Legarth (2004). One is an aluminium alloy Al 7108-T7 for which Moen et al. (1998) (see also Legarth et al., 2002a,b) used a fitting in terms of Hill-48. Here, in the yield function (2.13) the parameter values used are

$$F = 0.699, \quad G = 3.33, \quad H = 1, \quad N = 9.60 \tag{3.1}$$

Additional material parameters, used to fit a uniaxial tensile test with only $\sigma_{11} \neq 0$, are $\sigma_0/E = 0.003$, $\varepsilon_0 = 0.005$, $\nu = 0.3$, $n = 0.1$, $m = 0.005$ and $\dot{\Phi}_0 = 0.002s^{-1}$. In the traction–separation law the values $\delta_{\mathrm{n}}^c/\delta_{\mathrm{t}}^c = 1$, $\delta_{\mathrm{n}}^c = 0.1\Delta_0$, $\lambda_1 = 0.15$ and $\lambda_2 = 0.50$ are used, while $\hat{\sigma}/\sigma_0$ is varied.

The other material is an aluminium alloy Al 2090-T3 modelled by Legarth (2004) in terms of Barlat-91. In the yield function (2.14)–(2.19) the following parameter values are used

$$\bar{a} = 1.3392, \quad \bar{b} = 1.1650, \quad \bar{c} = 0.8111, \quad \bar{h} = 1.2262 \quad \text{and} \quad d = 8 \tag{3.2}$$

The additional material parameters used in this case are the same as those listed below (3.1), so that for uniaxial tension with only $\sigma_{11} \neq 0$ the same stress–strain curve is modelled.

The parameter identification for the two yield functions given above in (3.1) and (3.2) has been described in detail by Moen et al. (1998) and Legarth and Kuroda (2004), the latter based on experiments presented in Barlat et al. (2003). In Barlat et al. (2003) the yield stresses have only been shown normalized by that in the rolling direction. Therefore, in the present studies we have chosen to use the same value, $\sigma_0/E = 0.003$, for both materials. For the strain hardening, strain rate sensitivity and traction–separation law we do not have experimentally determined values in the present study. Therefore, reasonable values have been chosen, and in this respect the analyses here represent a parametric study.

For the two materials, plane strain tension in the x_1-direction has been used by Tvergaard and Legarth (2004) to illustrate the variation of the plane strain yield stress in the x_1-direction with the initial angle of orientation of the anisotropy. In both cases the lowest yield stress was found for the orientation $\theta_0 = 45°$, and it was also found that for Al 2090–T3 (Barlat-91) the yield stress never exceeds the isotropic von Mises yield stress, whereas Al 7108-T7 (Hill-48) depicts a yield stress above as well as below the isotropic yield stress.

Fig. 4 shows crack growth resistance curves for the Hill-48 material, with the parameter values specified by (3.1), where Δa denotes the length of the crack growth. The angle of inclination of the crack plane relative to the principal axis of anisotropy is taken to be $\theta_0 = 45°$, and the value of the peak stress to flow stress ratio is taken to be, $\hat{\sigma}/\sigma_0 = 3.25$. These curves are compared with corresponding curves for the Mises material. In both cases the crack growth resistance curves have been calculated for the materials with the

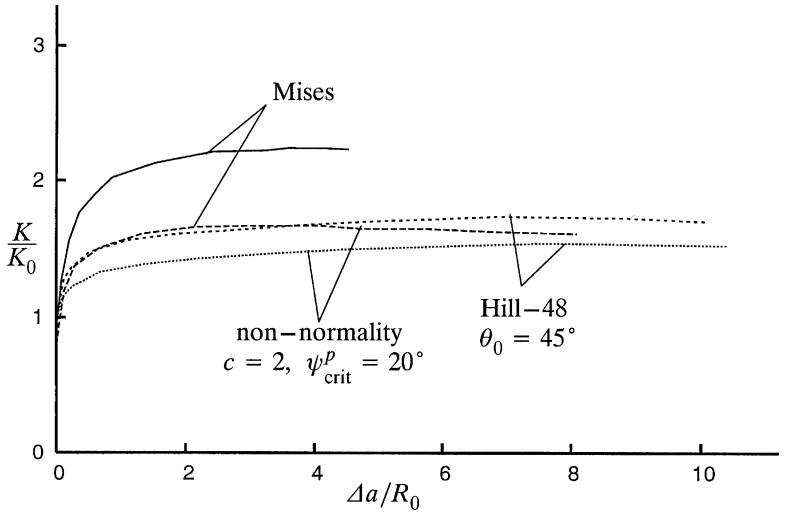

Fig. 4. Interface crack growth resistance curves for the Hill-48 material, Eq. (2.13), with $\hat{\sigma}/\sigma_0 = 3.25$ and $\theta_0 = 45°$, for normality of plastic flow and for the non-normality flow rule. Corresponding curves for Mises material are shown for comparison.

normality flow rule, as well as for non-normality with $c = 2$ and $\psi^{\text{p}}_{\text{crit}} = 20°$. Both for the Hill-48 materials and for the Mises materials the curves in Fig. 4 show that the maximum levels of fracture toughness on the resistance curves are reduced when the non-normality flow rule is applied. Furthermore, the curves for the Mises materials are above those for Hill-48.

Fig. 5 shows similar crack growth resistance curves for $\theta_0 = 0°$ and $\theta_0 = 90°$, where crack growth occurs parallel to one of the orthotropic axes. Again, the curves for the Mises material are included for comparison. It is seen that $\theta_0 = 90°$ leads to higher toughness levels than those found for $\theta_0 = 0°$, and in both cases the toughness levels are above those found for $\theta_0 = 45°$, as is seen by comparison with Fig. 4. Also in the cases of Fig. 5 the fracture toughnesses predicted for the normality flow rule are higher than those for non-normality.

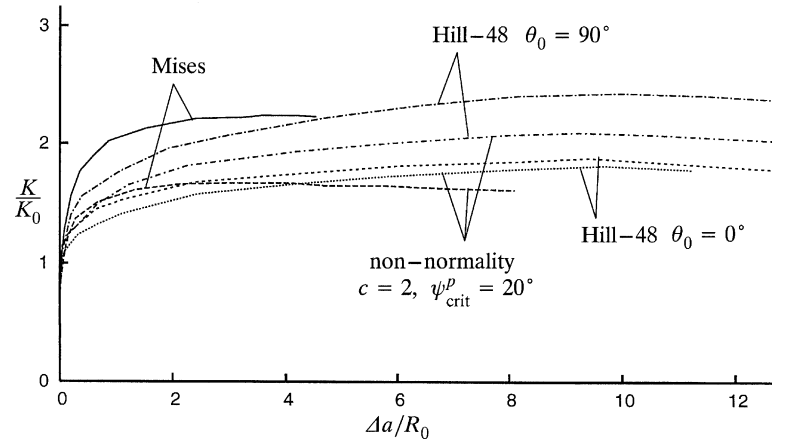

Fig. 5. Interface crack growth resistance curves for the Hill-48 material, Eq. (2.13), with $\hat{\sigma}/\sigma_0 = 3.25$ and $\theta_0 = 0°$ or $\theta_0 = 90°$. Corresponding curves for Mises material are shown for comparison.

It is assumed in the present computations that the growing crack remains in the initial crack plane, even though the stress and strain fields near the crack-tip are not generally symmetric for any value of θ_0. However, for $\theta_0 = 0°$ and for $\theta_0 = 90°$ there is exact symmetry, and for $\theta_0 = 45°$ the plastic regions are essentially symmetric, so in the cases considered here the assumption of straight ahead crack growth is not unreasonable.

The limiting value of K attained as the crack grows to approach a steady-state is denoted K_{ss}. Some of the predicted resistance curves go slightly downwards after reaching the maximum, so that in these cases K_{ss} is approached from above. However, as in the previous studies, the values K_{ss} are here identified as the peak values of the resistance curves. In Fig. 6 the dependence of K_{ss}/K_0 on the value of $\hat{\sigma}/\sigma_0$ is shown for cases corresponding to the four resistance curves in Fig. 4, where the resistance curves are plotted for the value $\hat{\sigma}/\sigma_0 = 3.25$. It is seen in Fig. 6 that the steady-state fracture toughnesses for the normality flow rule remain higher or practically identical to those for non-normality in the whole range studied. Furthermore, for increasing values of $\hat{\sigma}/\sigma_0$, the steady-state fracture toughnesses corresponding to the Mises material grow well above those for the Hill-48 material.

Similar curves for the dependence of K_{ss}/K_0 on the value of $\hat{\sigma}/\sigma_0$ are shown in Fig. 7 for cases corresponding to the six resistance curves in Fig. 5. The behaviour observed is mostly analogous to that in Fig. 6, but a noticeable difference is that in the case of Hill-48 with $\theta_0 = 0°$ the curve for the non-normality flow rule is a little above that for normality in a rather broad interval. It is also noted that the curve for $\theta_0 = 0°$ with normality grows well above that for $\theta_0 = 90°$ with non-normality in the range of larger values of $\hat{\sigma}/\sigma_0$.

The calculated resistance curves depend on the rate of loading, since the material is described as elastic–viscoplastic. In the initial parts of the resistance curves the rate of increase of the stress intensity factor K is taken to be $\dot{K} = K_0/t_R$, where t_R is a reference time. When the resistance curve flattens out, approaching the maximum value of K, the value of $\dot{K}$ will have to approach zero, so in this range the rate of crack growth is

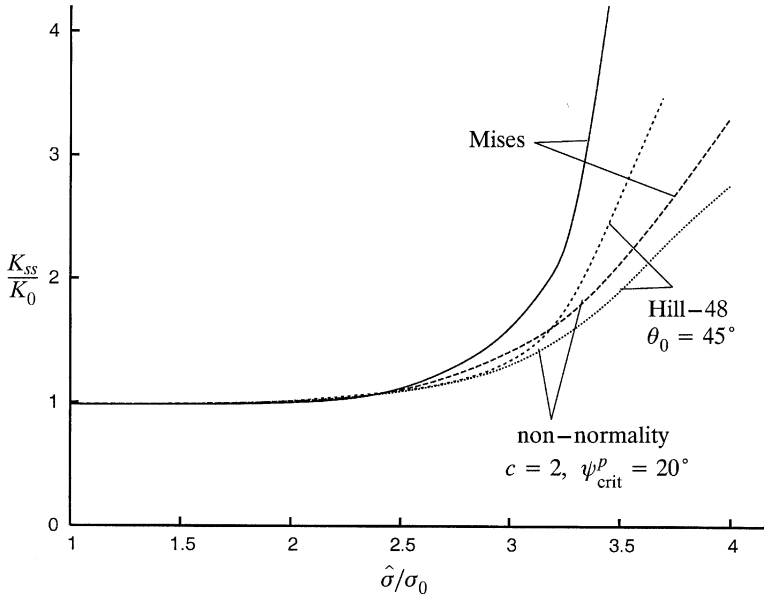

Fig. 6. Steady-state interface toughness vs. peak stress in the cohesive zone model for the Hill-48 material, Eq. (2.13), when $\theta_0 = 45°$. Corresponding curves for Mises material are included for comparison.

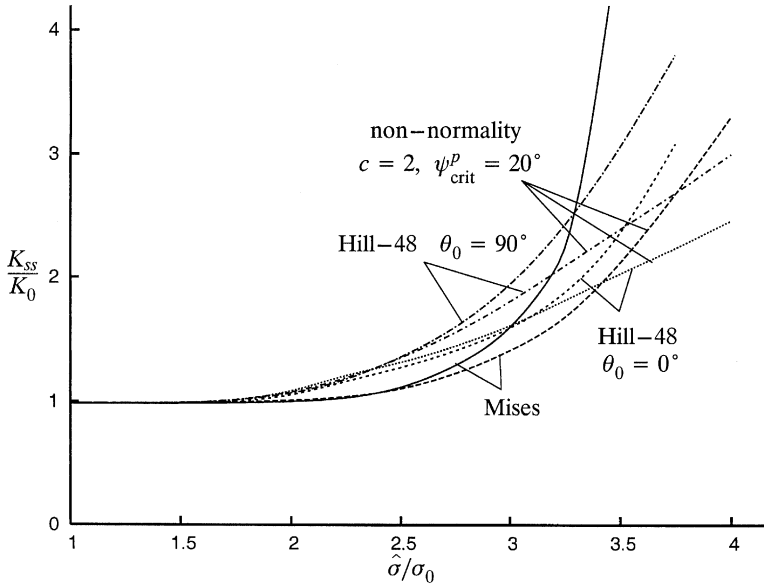

Fig. 7. Steady-state interface toughness vs. peak stress in the cohesive zone model for the Hill-48 material, Eq. (2.13), when $\theta_0 = 0°$ or $\theta_0 = 90°$. Corresponding curves for Mises material are included for comparison.

specified such that the rate of crack opening at the crack-tip is $\dot{\delta}_n = \delta_n^c/t_R$. In the present computations the value of the reference time is chosen as $t_R = 0.2/\dot{\Phi}_0$. For the low value of the rate-hardening exponent m applied here it is found that the sensitivity to the value of t_R is quite small.

The length ℓ of the fracture process region in the cohesive zone during crack growth may be characterized by the distance from the crack-tip, where $\lambda = 1$ in Fig. 2, to the point ahead of the crack-tip where $\lambda = \lambda_1$. Good resolution and very little mesh dependence is found when the value of ℓ is several times the length Δ_0 of a square element in the uniform mesh region (Fig. 3b). This requirement is satisfied in the present computations.

The sensitivity to the values of the parameter c or the angle ψ^{p}_{crit} is studied in Fig. 8, where two of the curves are identical to the curves for Hill-48 shown in Fig. 6. For $c = 2$ it is seen that a reduced value of the critical angle, $\psi^{p}_{crit} = 10°$, gives higher fracture toughness, more like that found for the normality flow rule, while an increased value, $\psi^{p}_{crit} = 30°$, gives lower fracture toughness. For $c = 0$ the direction of the plastic strain rate would coincide with the deviatoric value of the total strain rate, according to (2.10) and (2.11), while increased values of c allow for larger deviations between these directions. In Fig. 8, for $\psi^{p}_{crit} = 20°$ a comparison is made between predictions for $c = 2$ and $c = 4$, and it is found that the increased value gives only slightly lower fracture toughness.

Resistance curves have also been computed for the Barlat-91 material, with the parameter values specified by (3.2), and with focus on $\theta_0 = 45°$, as in Fig. 4. Based on these results Fig. 9 shows the variation of the steady-state values K_{ss}/K_0 vs. the peak stress, $\hat{\sigma}/\sigma_0$, in the traction separation law. As in Fig. 6 the steady-state toughnesses are shown both for the normality flow rule and for non-normality with $c = 2$ and $\psi^{p}_{crit} = 20°$, and also here results for the Mises material are included for comparison. As was also found by Tvergaard and Legarth (2004), the Barlat-91 material shows generally a higher toughness than that found for the Mises type material, at a given value of $\hat{\sigma}/\sigma_0$, whereas the trend is the opposite for Hill-48 in Fig. 6. This was explained by the fact that in uniaxial plane strain tension in different directions the Hill-48 material yields at stresses that are mostly higher than that for the Mises material, while the

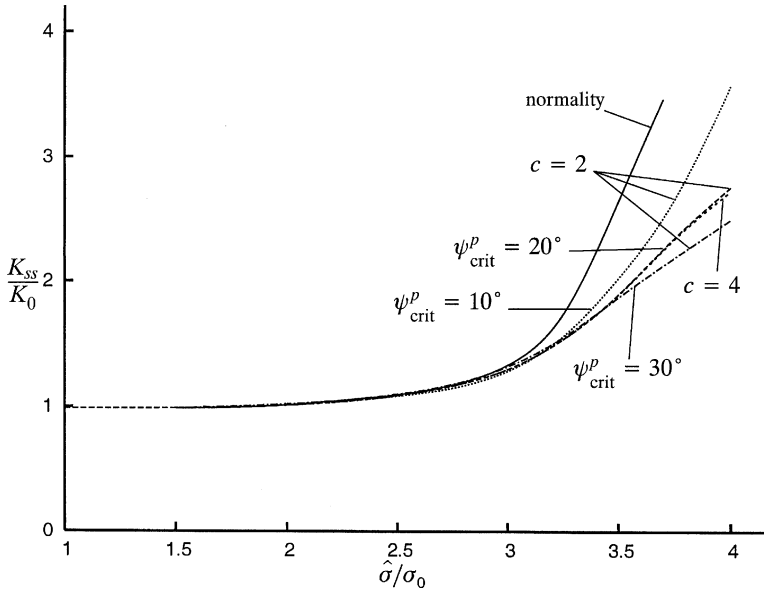

Fig. 8. Steady-state interface toughness vs. peak stress in the cohesive zone model for the Hill-48 material, Eq. (2.13), when $\theta_0 = 45°$. Comparison of predictions for different values of the angle ψ^p_{crit} and the parameter c in (2.11).

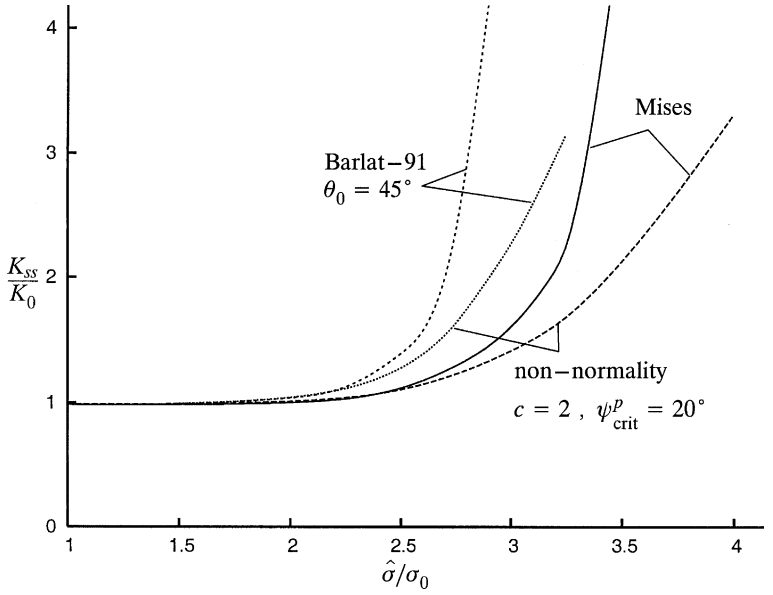

Fig. 9. Steady-state interface toughness vs. peak stress in the cohesive zone model for the Barlat-91 material, Eqs. (2.14)–(2.19), when $\theta_0 = 45°$. Corresponding curves for Mises material are included for comparison.

Barlat-91 material yields at stresses that are mostly lower. As in the previous figures the fracture toughnesses predicted by the non-normality flow rule are lower than those for normality.

4. Discussion

The non-normality flow rule for an anisotropic solid with a smooth yield surface, proposed by Kuroda and Tvergaard (2001a), was shown to give good agreement with predictions of polycrystal plasticity, where a vertex-type flow rule governs. For predictions of plastic instabilities a vertex has a big effect and it was shown, both for failure by necking in biaxially stretched metal sheets and for shear band development under plane strain conditions (Kuroda and Tvergaard, 2001b), that the phenomenological model with non-normality represents this effect. Crack growth in a ductile material is another case where a vertex-type flow rule is expected to have a large effect, since the movement of the crack-tip plastic zone during crack extension gives rise to significant deviations from a proportional stress history. Based on J_2 corner theory (Christoffersen and Hutchinson, 1979) the reduced resistance to non-proportional deformation in the case of a vertex has been studied by Dean and Hutchinson (1980). They considered crack growth under Mode III conditions and found different effects of the vertex when a critical strain criterion or a crack-tip opening criterion was used for crack growth.

The traction–separation law used here to model the fracture process gives a stress based crack growth criterion and thus differs from the criteria discussed by Dean and Hutchinson (1980). It is found that at practically all the parameter values considered the non-normality flow rule gives a smaller value of the steady-state fracture toughness K_{ss} than that found using standard normality. First of all, this effect is shown by the Mises material results, which are included in the figures for comparison with the curves predicted for plastic anisotropy. But with anisotropy the same tendency is found both for the Hill-48 material and the Barlat-91 material, except for a few parameter intervals, where the differences are rather small between the fracture toughnesses with or without normality of plastic flow. Thus, the conclusion based on the present crack growth model is that the strongly non-proportional stressing inherently involved in crack growth gives less fracture toughness when the constitutive model applied is less resistant to non-proportional deformation.

The sensitivity to the maximum angle of deviation ψ^{p}_{crit} from normality has been tested in Fig. 8 for the Hill-48 material. Consistent with the tendencies mentioned above, it is found that the reduction of the fracture toughness below that found for the normality flow rule is larger the larger the value of ψ^{p}_{crit}.

The cases analysed here are for crack growth parallel to the principal axes of the anisotropy, i.e. for $\theta_0 = 0^\circ$ and $\theta_0 = 90^\circ$ where there is exact symmetry, or for $\theta_0 = 45^\circ$ where the plastic regions are close to symmetric (Legarth et al., 2002a). Therefore, the assumption that the cracks grow straight ahead is assumed to give a good approximation in the cases studied.

As has also been found in previous investigations (Tvergaard and Hutchinson, 1992, 1993) the predicted steady-state fracture toughness is very sensitive to the value of the peak stress in the traction separation law, i.e. to the value of the ratio $\hat{\sigma}/\sigma_0$. Furthermore, the curves for the steady-state fracture toughness K_{ss}/K_0 vs. $\hat{\sigma}/\sigma_0$ confirm that, as long as $\hat{\sigma}/\sigma_0$ is so small that plasticity at the crack-tip plays only a minor role, the fracture toughness depends only on the local work of separation Γ_0 on the crack plane.

Acknowledgements

Assoc. Prof. Mitsutoshi Kuroda, Yamagata University, Japan is thanked for valuable comments.

This work is supported by the Danish Technical Research Council in a project on Anisotropic Plasticity under the Materials Research Programme.

References

Barlat, F., Lege, D.J., Brem, J.C., 1991. A six-component yield function for anisotropic materials. Int. J. Plast. 7, 693–712.

Barlat, F., Maeda, Y., Chung, K., Yanagawa, M., Brem, J.C., Hayashida, Y., Lege, D.J., Matsui, K., Murtha, S.J., Hattori, S., Becker, R.C., Makosey, S., 1997. Yield function development for aluminum alloy sheets. J. Mech. Phys. Solids 45, 1727–1763.

Barlat, F., Brem, J.C., Yoon, J.W., Chung, K., Dick, R.E., Lege, D.J., Pourboghrat, F., Choi, S.-H., Chu, E., 2003. Plane stress yield function for aluminum alloy sheets—part I: Theory. Int. J. Plast. 19, 1297–1319.

Christoffersen, J., Hutchinson, J.W., 1979. A class of phenomenological corner theories of plasticity. J. Mech. Phys. Solids 27, 465–487.

Dean, R.H., Hutchinson, J.W., 1980. Quasi-static steady crack growth in small-scale yielding. Fracture Mechanics: Twelfth Conference, ASTM STP 700. American Society for Testing and Materials, pp. 383–405.

Hershey, A.V., 1954. The plasticity of an isotropic aggregate of anisotropic face centered cubic crystals. Trans. ASME, J. Appl. Mech. 21, 241–249.

Hill, R., 1948. A theory of the yielding and plastic flow anisotropic metals. Proc. Roy. Soc. London A 193, 281–297.

Hill, R., 1950. The Mathematical Theory of Plasticity. The Clarendon Press, Oxford.

Hosford, W.F., 1972. A generalized isotropic yield criterion. Trans. ASME, Series E, J. Appl. Mech. 39, 607–609.

Kuroda, M., Tvergaard, V., 1999. Use of abrupt strain path change for determining subsequent yield surface: Illustrations of basic idea. Acta Mater. 47, 3879–3890.

Kuroda, M., Tvergaard, V., 2000. Forming limit diagrams for anisotropic metal sheets with different yield criteria. Int. J. Solids Struct. 37, 5037–5059.

Kuroda, M., Tvergaard, V., 2001a. A phenomenological plasticity model with non-normality effects representing observations in crystal plasticity. J. Mech. Phys. Solids 49, 1239–1263.

Kuroda, M., Tvergaard, V., 2001b. Plastic spin associated with a non-normality theory of plasticity. Eur. J. Mech. A Solids 20, 893–905.

Kuroda, M., Tvergaard, V., 2001c. Shear band development predicted by a non-normality theory of plasticity and comparison to crystal plasticity. Int. J. Solids Struct. 38, 8945–8960.

Kuwabara, T., Kuroda, M., Tvergaard, V., Nomura, K., 2000. Use of abrupt strain path change for determining subsequent yield surface: Experimental study with metal sheets. Acta Mater. 48, 2071–2079.

Legarth, B.N., 2003. Debonding of particles in anisotropic materials. Int. J. Mech. Sci. 45, 1119–1133.

Legarth, B.N., 2004. Unit cell debonding analyses for arbitrary orientations of plastic anisotropy. Int. J. Solids Struct. 41, 7267–7285.

Legarth, B.N., Kuroda, M., 2004. Particle debonding using different yield criteria. Eur. J. Mech. A Solids 23, 737–751.

Legarth, B.N., Tvergaard, V., Kuroda, M., 2002a. Effects of plastic anisotropy on crack-tip behaviour. Int. J. Fracture 117, 297–312.

Legarth, B.N., Tvergaard, V., Kuroda, M., 2002b. Crack-tip blunting in an anisotropic material with plastic spin. On-line publication of WCCM V—Fifth World Congress on Computational Mechanics, ISBN 3-9501554-0-6. http://wccm.tuwien.ac.at/.

McMeeking, R.M., Rice, J.R., 1975. Finite-element formulations for problems of large elastic–plastic deformation. Int. J. Solids Struct. 11, 601–616.

Moen, L.A., Langseth, M., Hopperstad, O., 1998. Elastoplastic buckling of anisotropic aluminum plate elements. J. Struct. Eng., 712–719.

Nagtegaal, J.C., Parks, D.M., Rice, J.R., 1974. On numerically accurate finite element solutions in the fully plastic range. Comput. Methods Appl. Mech. Eng. 4, 153–177.

Needleman, A., 1987. A continuum model for void nucleation by inclusion debonding. J. Appl. Mech. 54, 525–531.

Simo, J.C., 1987. A J2-flow theory exhibiting a corner-like effect and suitable for large-scale computation. Comput. Methods Appl. Mech. Eng. 62, 169–194.

Tvergaard, V., 1976. Effect of thickness inhomogeneities in internally pressurized elastic–plastic spherical shells. J. Mech. Phys. Solids 24, 291–304.

Tvergaard, V., 1990. Effect of fibre debonding in a whisker-reinforced metal. Mater. Sci. Eng. A 125, 203–213.

Tvergaard, V., 2001. Resistance curves for mixed mode interface crack growth between dissimilar elastic–plastic solids. J. Mech. Phys. Solids 49, 2689–2703.

Tvergaard, V., Hutchinson, J.W., 1992. The relation between crack growth resistance and fracture process parameters in elastic–plastic solids. J. Mech. Phys. Solids 40, 1377–1397.

Tvergaard, V., Hutchinson, J.W., 1993. The influence of plasticity on mixed mode interface toughness. J. Mech. Phys. Solids 41, 1119–1135.

Tvergaard, V., Legarth, B.N., 2004. Effect of plastic anisotropy on crack growth resistance under mode 1 loading. Int. J. Fracture 130, 411–425.

Yamada, Y., Hirakawa, H., 1978. Large deformation and instability analysis in metal forming process. Appl. Numer. Methods Form. Process., ASME, AMD 28, 27–38.

Yamada, Y., Sasaki, M., 1995. Elastic–plastic large deformation analysis program and lamina compression test. Int. J. Mech., 691–707.